UNIVERSITÀ DEGLI STUDI DI PADOVA

Dipartimento di Fisica e Astronomia "Galileo Galilei"

Corso di Laurea in Fisica

Tesi di Laurea

Study heavy elements with exotic beams at ISOLDE (CERN)

Relatore

Dott. Jose Javier Valiente Dobon

Correlatore

Dott. Andrés Illana Sisón

Laureando

Marco Bortolami

Anno Accademico 2017/2018

Contents

Abstract

Nuclear structure physics has, as a main objective, the study of the nature and the phenomenology of nucleon-nucleon interaction. In the same way than the atoms, nuclear structure can be explained in term of shells (different for protons and neutrons) and the regions around double-shell closures are a benchmark for the study of nuclear structure since they are a direct source of information on the nucleon-nucleon effective interaction in nuclei. Furthermore, these regions are useful to study experimentally since they can be easily described by the nuclear shell model. There are several cases in nature of doubly-magic nuclei but the heaviest known is the ^{208}Pb nucleus. In particular, the south-east region around ^{208}Pb is difficult to study due to experimental limitations such as low cross-section production and limits in the performance of the detectors for such heavy nuclei, so it has not been thoroughly explored so far [1, 2]. Multi-Nucleon Transfer (MNT) reactions are a valid process to produce neutron-rich nuclei around ^{208}Pb and gamma-ray spectroscopy represents one of the most powerful methods to study nuclear structure since a large fraction of the de-excitation of the excited nuclear levels goes via gamma emission [3].

This work will focus on the gamma-ray spectroscopy study of the beam-like and target-like products of a MNT reaction induced via a radioactive ^{94}Rb beam impinging on a ^{208}Pb target. In particular, the cases of ^{94}Zr and ^{210}Pb will be discussed. In the first chapter, the atomic nucleus and different reaction mechanisms used for the production of exotic nuclei, in particular around ^{208}Pb, will be introduced. The second chapter will focus on the experimental facility where the experiment was performed and the setup used for it, for example the gamma and particle detectors. The following two chapters, called "Pre-sorting of the data" and "Data analysis", will discuss the first steps performed for the analysis of the data, the study of the β contaminants, the decay of ^{94}Y into ^{94}Zr, which is one of the the major components of the background, and the ^{210}Pb. In the last chapter, "Conclusions and future perspectives", the summary of the results and the conclusions obtained in this thesis will be reported, as well as an introduction to the following experiment.

Chapter 1

Introduction

1.1 The atomic nucleus

An atom is a bound system of non-fundamental particles formed by a core, namely the nucleus, and surrounded by a cloud of electrons. The nucleus is made of two types of nucleons: the protons, whose number is Z, and the neutrons, whose number is N. The sum of the atomic number, Z, and of the number of neutrons, N, gives the mass number, A. These values define a specific nucleus. As an example, the ^{210}Pb nucleus has A = 210 nucleons (Z = 82 protons and N = A − Z = 128 neutrons). Almost all the matter of an atom is concentrated in the nucleus. However, the nuclear and atomic radii are of the order of 10^{-15} m and 10^{-10} m, respectively.

When one deals with the nuclei, the forces that matter are not all the four fundamental forces, namely the gravity, strong, weak and electromagnetic forces. In fact, the force of gravity is negligible with respect to the other three, and it does not play a role in the nuclear structure nor in the nuclear reactions. On the other hand, the strong force is the one that binds together the nucleons and it is responsible of the alpha decay, which is an emission of a ^{4}He nucleus (two protons and two neutrons) in order to become a different nucleus with A − 4 nucleons. The beta decays, instead, are governed by the weak force, that causes the emission of a beta particle (which is an electron for the β^- decay and a positron for the β^+ one) and an (anti)neutrino while transforming a neutron into a proton or vice-versa: a specific nucleus changes after this decay, also, as Z and N are not the same before and after the reaction. Another similar process in competition with the β^+ decay is the electron capture: an electron that passes near the nucleus can be captured by a proton and the two change into a neutron and the emission of a neutrino. Finally, the electromagnetic force is responsible of the gamma decay, where a nucleus in an excited state decays into a lower state via the emission of a gamma ray with an energy equal to the difference between the ones of the two states related to the transition. [4]

It is very well known that the various elements in the Mendeleev's periodic table are distinguishable by the number of protons, but each of them can show itself with a different number of neutrons: these nuclei with the same Z but different N are called isotopes. For this reason in nuclear physics is necessary to present the nuclei in a different way. The Segré chart, or chart of nuclides, is a collection of all the isotopes in a graph reporting the number of protons on the ordinates, the number of neutrons on the abscissas and eventually another property, such as the mean lifetime or the most likely way of decay, using different colors for the points. An example of this chart is shown in figure 1.1, where the color distinguish if a nucleus is stable, unstable and was observed or unstable and has not been observed yet. The unstable isotopes, in most of the cases, try to reach the valley of stability (as the black "line" is called) by alpha, beta decays, electron capture, fission and other processes. As one goes away from the valley, there is more and more difficulty in creating such nuclei. A lot of work was (and is) performed to fill the empty parts of the chart of nuclides: many experiments have been carried out in order to produce the most exotic nuclei far from the stability.

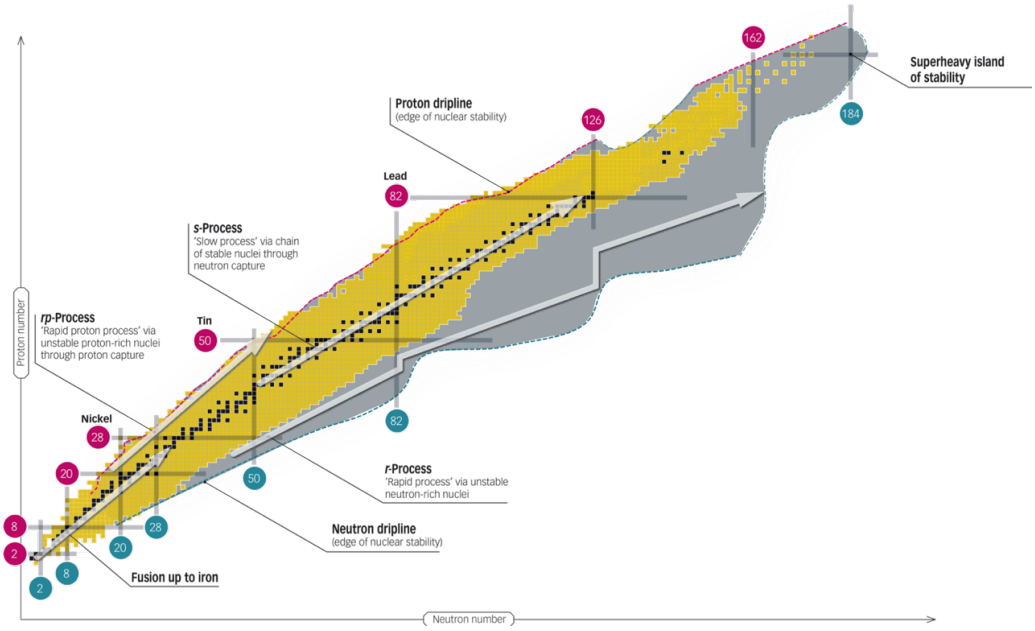

Figure 1.1: the chart of nuclides, showing the stable (in black) and the unstable nuclei. These latter are divided into nuclei that were discovered (in yellow) and those we do not know yet (in gray). The latter region is named "terra incognita". The proton (in red) and neutron (in blue) driplines are drawn. The magic numbers are shown in the circles.

1.2 The shell model

There are many models in nuclear physics that describe the behavior of the nucleons inside the nucleus and the shell model is one of them. It well reproduces the discrete states occupied by the nucleons, each one related to a specific orbital. The orbitals are filled with the nucleons and when a shell is complete there is a high stability. This condition is called shell closure and it happens at certain numbers, called magic numbers, that are 2, 8, 20, 28, 50, 82, 126. If a nucleus has a magic number of protons or neutrons, it is called "semi magic nucleus" and if it has a magic number of both protons and neutrons, it is called "double magic nucleus" [5].

It is useful to show some examples of behaviors that point out the presence of them. If a plot of the energy necessary to separate a proton or a neutron from the nucleus versus the number of protons or neutrons respectively is made, it can be clearly seen that the quantity on the ordinates has a peak for Z or N equal to these numbers: this is related to a shell closure, that makes more difficult the extraction of a nucleon because of the higher stability. Not only the loss of nucleons, but also the gain of them is altered: the cross section for neutron absorption in correspondence of the magic numbers is lower than the one at near numbers of neutrons, as it is shown in figure 1.2.

Therefore, there is the necessity of a model that describes these behaviors. The Schrödinger equation has to be solved: in this case it is a single particle equation (a nucleon in general), which moves in a mean nuclear field represented by the potential $V(r)$. Since the field is supposed to be central, it is true that $V(r) = V(|r|)$. The equation mentioned above is equation 1.1:

$$-\frac{\hbar^2}{2m}\nabla^2\Psi(\mathbf{r}) + V(r)\Psi(\mathbf{r}) = E\Psi(\mathbf{r}) \tag{1.1}$$

Different approximations for the potential can be performed, each one representing some properties of the nucleus: for example, an harmonic potential or a potential square well can be used, the latter describing the short range of the strong force. However, these choices lead to conclusions that are not in agreement with the experimental results: the numbers of particles at which the shells close are not the same for experiments and theoretical calculations. It is possible to reproduce the data, for

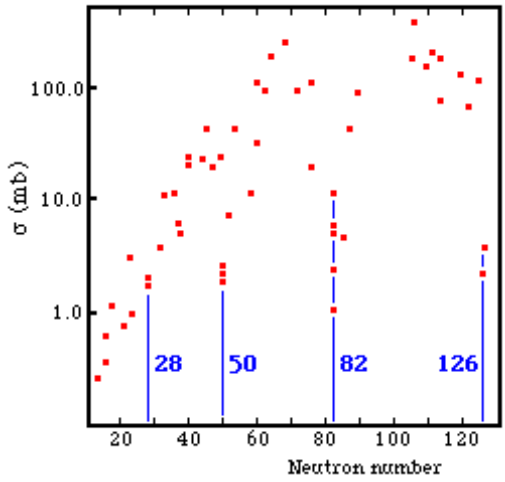

Figure 1.2: Graph showing the cross section for neutron absorption (in mb and logarithmic scale) versus the number of neutrons N. Some magic numbers are shown. Image taken from [6].

example, using the spin-orbit potential:

$$V_{\mathbf{L}\cdot\mathbf{S}}(r) = k\frac{dV(r)}{dr}\mathbf{L}\cdot\mathbf{S}, \tag{1.2}$$

where k is a constant, $\mathbf{L}\cdot\mathbf{S}$ is the scalar product of the orbital angular momentum and the spin momentum and $V(r)$ is the Woods-Saxon potential

$$V(r) = \frac{V_0}{1+e^{-\frac{r-r_0}{a}}}; \tag{1.3}$$

in the last equation V_0 is the depth of the well, r_0 is the radius at half height and a is is the diffusivity parameter. Other choices for $V_{\mathbf{L}\cdot\mathbf{S}}(r)$ can be made.

This $V_{\mathbf{L}\cdot\mathbf{S}}(r)$ separates the two cases with total angular momentum $\mathrm{J} = |\mathrm{L} - \mathrm{S}|$ and $\mathrm{J} = \mathrm{L} + \mathrm{S}$, where L is the modulus of the orbital angular momentum and S=1/2 is the modulus of the spin. With this simple interpretation it is possible to reproduce the magic numbers and to estimate the position of the levels [7, 8]. A scheme of the states fillable by the particles, predicted by using the spin-orbit potential, is shown in figure 1.3. By composing all the momenta of the particles, the total angular momentum and parity J^π can be obtained. To have better results, a distinction between protons and neutrons can be done using different potentials that take care, for example, of the coulombian interaction between protons [9]. If the nucleus is excited or de-excited (via gamma decay), the nucleons change level, so the energy and J^π of the system: a level scheme based on these quantities can be created. These schemes will be used in the following.

1.3 Reaction mechanisms and gamma spectroscopy

Gamma spectroscopy is crucial for the comprehension of the nuclear structure. Via this technique we can extract many information like: the energy of the states and of the transitions between them; the lifetime of an excited state, that can give us the reduced transition matrix elements; the angular distributions, which can let us understand the multipolarity of the transition; the polarisation, that can provide information on the electric or magnetic character of the transition [3]; the total angular momentum and parity of a level. A wide variety of different nuclei was studied using gamma-ray spectroscopy.

In order to study the gamma rays emitted by a nucleus, it has to be produced and excited. Depending on what is the object of study, different reactions can be used to reach the own purposes. One reaction among many that are performed is the coulomb excitation: with this method a nucleon is excited below the coulomb barrier and it is possible to understand more about the spin of the

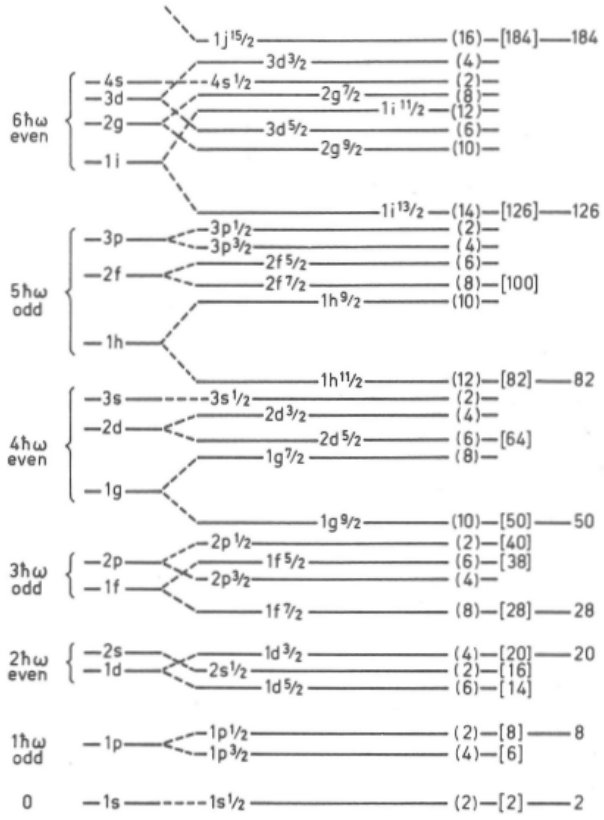

Figure 1.3: Levels predicted by the shell model using the spin-orbit potential [10, 11].

levels, the transitions matrix elements and the collective degrees of freedom (DOF). Going up with the energy, as soon as the coulomb barrier is surpassed the nucleons interaction starts to not be negligible. Therefore, the transfer reaction channels gain relevance. One nucleon transfer is a reaction that concerns single particle DOF, in fact a proton or a neutron is transferred from a nucleus to another. The evolution of shell structure, namely for example how the structure of the shell changes going from a magic nucleus to another maintaining the same Z, can be unraveled. Other reactions are elastic and deep inelastic scattering (a scattering where we have and do not have respectively the same nuclei before and after the process), fusion-evaporation (with which two nuclei are fused into one that then evaporates, namely emits, light particles like protons and neutrons in overabundance) or fission (a heavy nucleus is divided in two main fragments plus other lighter particles). Every reaction excite in a different way the nucleus of interest. Therefore, depending on the goals we are interested in, we should use one or another reaction [12].

Another important reaction mechanism, that provides the possibility to investigate exotic nuclei, is the multi-nucleon transfer reaction. It consists in a transfer of some nucleons from another nucleus. In general, the aspects that rule the transfer processes are the form factors, the dynamics of the reaction and the Q-value considerations, namely the balance of the internal and binding energy in the phase space of the colliding nuclei. The former expresses the process dependence from the nuclear structure, in particular from the initial and final wave functions of the transferred nucleons: if nuclear structure is the final result of the study subsequent a transfer experiment, then it is needed to perform it in a way that can enhance the dependence on the form factors. In fact, by varying where the detectors are positioned and their type, the importance of the elements that govern the reaction processes is different: various regimes are present.

In a multi-nucleon transfer reaction there is an angle in which the reaction cross-section is peaked, namely the grazing angle, $\theta_{grazing}$. At this angle the probability of detecting a particle coming from a MNT reaction is maximized. This is defined as the angle at which the distance of the closest approach equals the sum of the nuclear radii: this means that the two interacting nuclei are just *touching* each

other. The distance of the closest approach d is given by:

$$d = \left(\frac{Z_t Z_b e^2}{4\pi\epsilon_0 E_k}\right) \times \left(1 + csc\frac{\theta_{grazing}}{2}\right), \tag{1.4}$$

where Z_t and Z_p are the atomic numbers of the two nuclei involved in the reaction (t is used for the target nucleus and b for the beam one), e is the fundamental charge, ϵ_0 is the void dielectric constant, E_k is the kinetic energy and $\theta_{grazing}$ is the grazing angle. The sum of the two nuclear radii can be estimated by the usage of the Fermi radius:

$$d = 1.2\left(A_t^{1/3} + A_b^{1/3}\right) fm, \tag{1.5}$$

where A_t and A_b are the mass numbers of the two nuclei involved in the reaction. If equation 1.4 is compared with 1.5, the grazing angle can be estimated [3].

If the detector used in the transfer experiment is placed at this angle, two limit cases are possible. Firstly, if the ejectile excitation energy is higher than 20 MeV, the transferred nucleons are in a continuum of quantum states: there is not a dependence on form factors, but the dynamic factor dominates. Furthermore, there is a high transfer of energy because a large amount of kinetic energy is dissipated into internal excitation energies of the two emerging fragments. These reactions are called deep-inelastic reactions. If the ejectile excitation energy is lower than 20 MeV, instead, the transferred particles are in a discrete energy level: there is a high dependence on nuclear structure. In this case there is not a large loss of kinetic energy. These are the proper MNT reactions. These two regions are shown in figure 1.4.

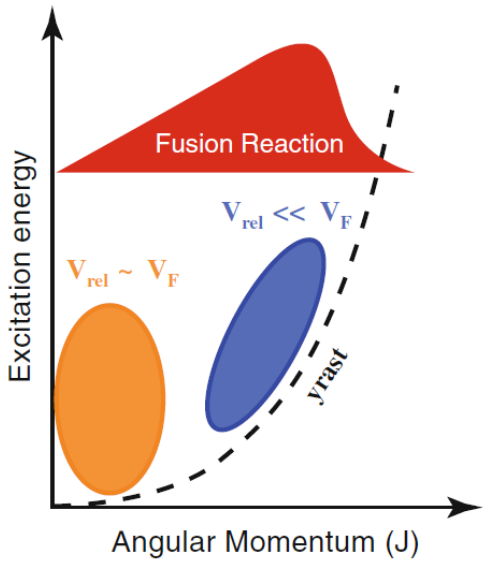

Figure 1.4: Schematic representation of the states populated in a graph reporting the excitation energy versus the angular momentum degrees of freedom, where v_{rel} and v_F are the relative and Fermi velocities respectively. The region of population for fusion-evaporation reactions is depicted for comparison. Image taken from [3].

Although these two processes are different, they are similar in some aspects: a projectile-like and a target-like particle are distinguishable due to the fact that the products of the reaction are similar to the initial nuclei, having only a few nucleons more or less than at the beginning; angular momentum is transferred from the relative orbital motion to the intrinsic spin of the two reaction products; the ejectiles de-excite through evaporation of neutrons, protons and α particles, through fission and, more interesting for the object of this work, through γ decay.

Another aspect that depends on the energy is the transfer of angular momentum. If the energy of the transfer reaction is close to the Coulomb barrier, so very small if compared to the Fermi kinetic energy, the angular momenta of the orbiting nucleons of the initial $\mathbf{l_i}$ and final $\mathbf{l_f}$ states would be perpendicular to the scattering plane and their projections would have opposite sign, while the spin $\mathbf{s_{i,f}}$ tends to keep its direction in the transfer process [3]. The maximum angular momentum

transferred is given by $l_{transfer} = |\mathbf{l_i} + \mathbf{l_f}| = |\mathbf{l_i}| + |\mathbf{l_f}|$. Instead, at higher energies, close to the Fermi kinetic energy, the relative angular momentum between the two nuclei is also higher and the final total angular momentum is $j_f = l_f \pm 1/2$.

The MNT reactions have been performed during the last decades with stable beams. This technique allows us to excite yrast and near yrast states, to understand different band structures and to study possible isomers and/or short lived states. Another advantage of this method is that several nuclei can be studied at the same time [2]. Instead of using stable beams like in the past, it is possible to use a Radioactive Ion Beam (RIB) for the multi-nucleon transfer reaction. Therefore, for example in the case of two neutrons pick up, in particular in the ^{210}Pb case, the yields expected will be higher and thus the statistics will be increased for a neutron-rich beam than using a stable beam. This is possible only if a high-intensity RIB can be produced and accelerated at the right energy. The production cross sections calculation for the reaction used in the experiment of this work, that is a ^{94}Rb beam impinging on ^{208}Pb, is shown in figure 1.5. It can be noticed that ^{210}Pb is part of the region with the highest values.

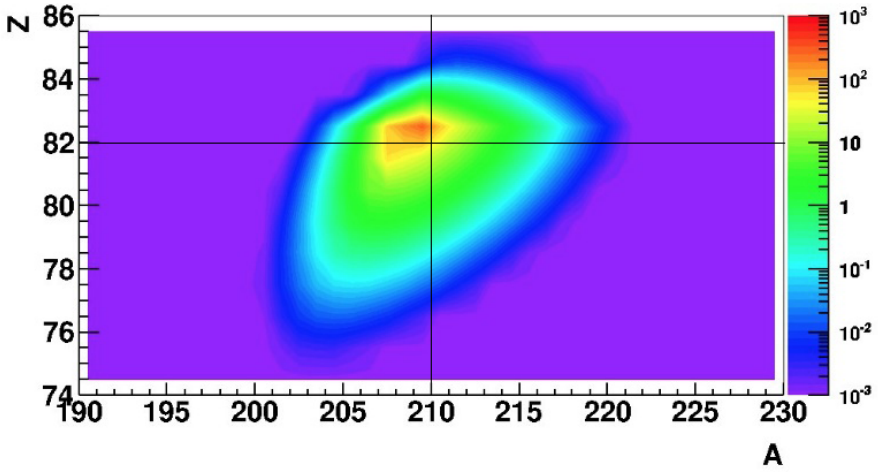

Figure 1.5: Calculations for the production cross sections of multi-nucleon transfer reactions as a function of the transferred protons and neutrons. The results refer to the collision of ^{94}Rb isotopes on ^{208}Pb at energies about 20% above the nominal Coulomb barrier. The position of the ^{210}Pb is shown. Image adapted from [1].

Chapter 2

The experiment

Different facilities across the world provides the possibility to use RIBs for the experiments: some examples are GSI in Germany, RIKEN in Japan, ALTO in France, TRIUMF in Canada and ISOLDE in Switzerland. This latter is where the experiment of the present work was conducted.

In general, there are two main methods to produce RIBs. The first is called in-flight method, which consists in a primary beam impinging on a thin target where the secondary beam is produced via fragmentation. All the particles are always in motion during the process. The second is the ISOL (Isotope Separator On-Line) method, in which a primary beam interacts with a thick target where the secondary products are stopped, ionized and extracted. A drawing of this method is shown in figure 2.1.

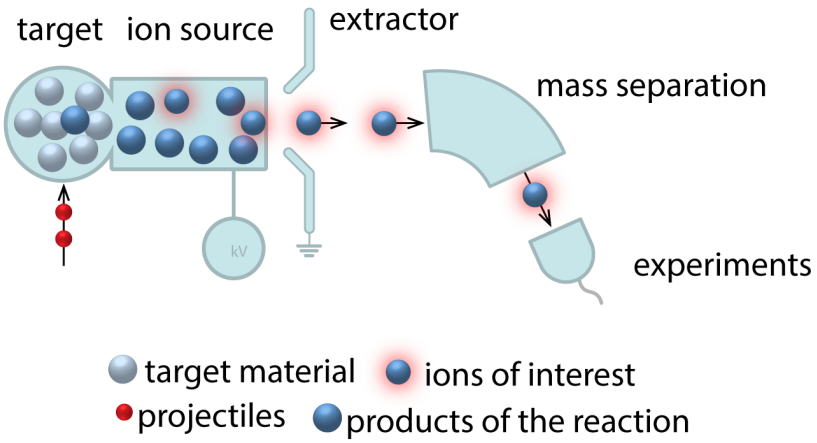

Figure 2.1: Schematic drawing of the processes needed to product the RIB via the ISOL method. In the target the projectiles create the primary products, which are then ionized, extracted and mass separated. The experimental chambers are reached at the end.

2.1 The ISOLDE facility

ISOLDE (Isotope Separator On-Line DEvice) is an ISOL facility at CERN, in Geneva. The most of the work done here is focused on nuclear physics. Figure 2.2 shows a drawing of ISOLDE. The part where RIB are produced via the ISOL method is flagged as "ISOLDE" in figure 2.2: the primary beam is made of protons having an energy of 1.4 GeV coming from the Proton-Synchrotron Booster (PSB), which is the preaccelator for the Large Hadron Collider (LHC). The atoms produced, made of ^{94}Rb for this experiment, are then ionized to 1^+ charge state and accelerated to 60 keV. The following step is REXTRAP, that is a Penning trap that accumulates, bunches and cools the ISOLDE quasi-continuous beam and performs charge-state breeding in order to optimize the transmission. Then there is REXEBIS, where an Electron Beam Ion Source (EBIS) achieves charge multiplication by electron bombardment. After the REXEBIS, the beam is released in bunches and injected in

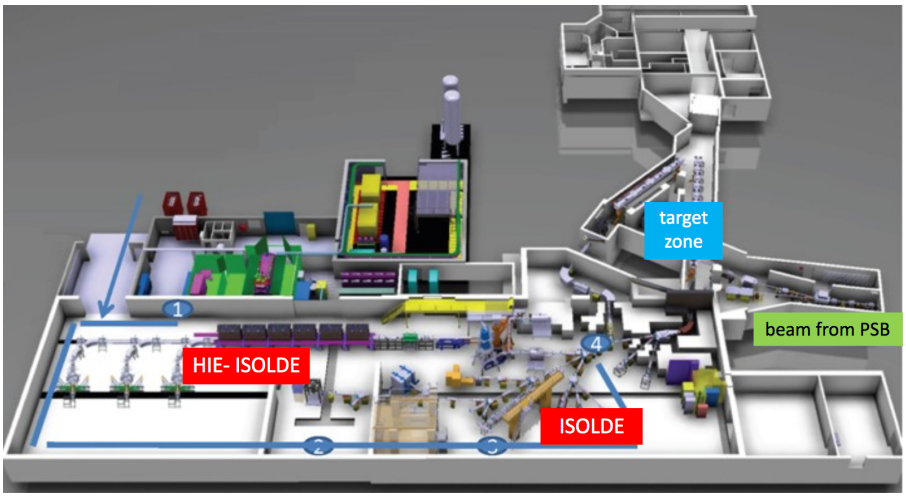

Figure 2.2: A drawing of the ISOLDE facility.

the post-accelerator system, called HIE-ISOLDE, via an A/q mass separator. This system, which is composed of normal RF cavities used in the previous system, called REX-ISOLDE, and 4 new cryo-cavities, can accelerate beams up to 10 MeV/u [13, 14]. At the time when this experiment was carried out only 3 out of 4 cryocavities were installed and running. The post-accelerated RIB is sent to different experimental areas and one of them is the MINIBALL setup. This part of ISOLDE is marked as HIE-ISOLDE in figure 2.2 [15, 16]. The experiment of the present work was performed at ISOLDE, with the MINIBALL setup, in September 2017.

2.2 The MINIBALL array

The MINIBALL array is made of 24 high-purity germanium crystals, each of them six-fold segmented so a better space resolution is provided; the 24 crystals are arranged in 8 clusters of 3 crystals each. Despite the six-fold segmentation, each crystal provides seven signals: six are from the outer parts and the last one is from the center and is the sum of the energy deposited in the whole crystal. The total setup, one single cluster and a drawing of one single crystal can be seen in figure 2.3.

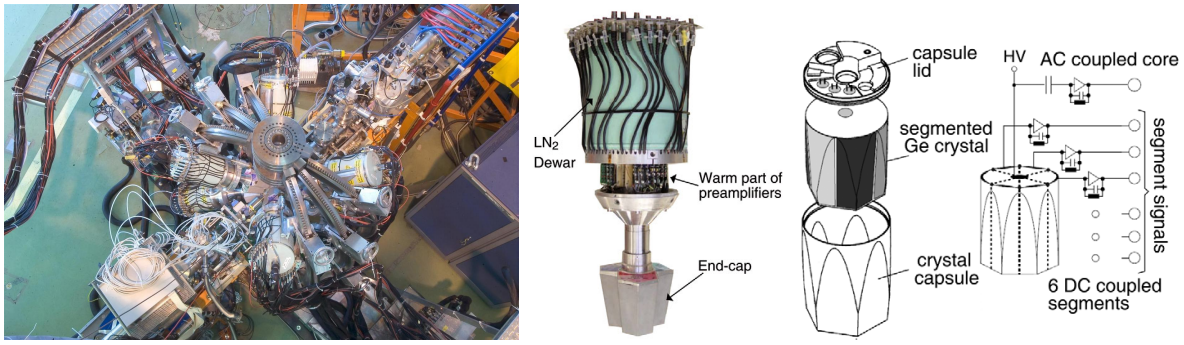

Figure 2.3: Left picture: the MINIBALL array. Image taken from [17]. Center picture: one of the 8 clusters that compose the setup. The preamplifiers are indicated and the crystals are flagged as "End-cap". Image taken from [18]. Right picture: Drawing of a MINIBALL detector. On the left the three main components (the capsule containing the crystal, the crystal and the lid) can be seen. On the right, the six-fold segmentation. Image taken from [18].

The Ge crystals are the hearth of the detector, as it is here that the gammas convert into electrons (via the processes explained in appendix A) that are collected and their signals are amplified and analyzed. The space tracking of the gamma particle is useful, when joined with the informations coming from the particle detectors, to have informations on if and which one of the particles detected emitted the gamma.

Due to the low multiplicity, having a good efficiency is an important feature when using radioactive

ion beams. For this reason, the Compton-suppression shields, devices capable of lowering the Compton background by removing the gammas that release only partially their energy in the detector, are absent in MINIBALL, in fact the cleaning of the spectra is outweighed by the loss in efficiency. However, there is the possibility to add them in a second moment, when higher beam energies become available at ISOLDE [18]. The data acquisition (DAQ) system for MINIBALL is synchronized with the EBIS signal from ISOLDE. It is used to start the measurement a few nanoseconds before the beam arrives at the MINIBALL target area and to measure during a certain time, which is correlated to the time structure of the beam. The structure of the data is specified in section 3.1.

2.3 Experimental details and setup

As it was mentioned in section 2.1, the ^{94}Rb was produced at ISOLDE using a standard UC_x as a primary target. The isotopes of interest were surface ionized and the yield production was more than 10^8 pps. After the extraction the beam was separated, bunched and accelerated up to 6.2 MeV/u. Unfortunately, due to radio-protection limitations inside the ISOLDE hall, the beam intensity was limited at 10^6 pps. This limitation was caused by the increase of radiation inside the hall as a consequence of the big amount of beam looses along the path. Therefore, the reduction in the beam intensity produced an impact in our physics case. Inside the reaction chamber, the ^{94}Rb RIB impinged on a pure ^{208}Pb target. Different channels were opened, but the specific MNT reaction searched for in the experiment consisted in the transfer of two neutrons from the nucleus of ^{94}Rb to the nucleus of ^{208}Pb, so:

$$^{94}\mathrm{Rb} + ^{208}\mathrm{Pb} \rightarrow ^{92}\mathrm{Rb} + ^{210}\mathrm{Pb} \tag{2.1}$$

Two different targets were used during the experiment: one thin target of 1 mg/cm^2 was used to understand the reaction mechanism and for cross-section calculations purpose, and one thick target of 13 mg/cm^2 to perform in-beam gamma-ray spectroscopy. The thickness of the thick target was chosen in order to stop all the lead-like particles inside the target after a MNT reaction and therefore all the γ rays related to the de-excitation of the lead-like nuclei will be emitted at rest, without Doppler effect. However, the partner nuclei, the rubidium-like, left the target. The detection of the rubidium-like particles was crucial because it reveals that a reaction happened inside of the target might be a MNT reaction. A representation of these mechanisms is shown in figure 2.4.

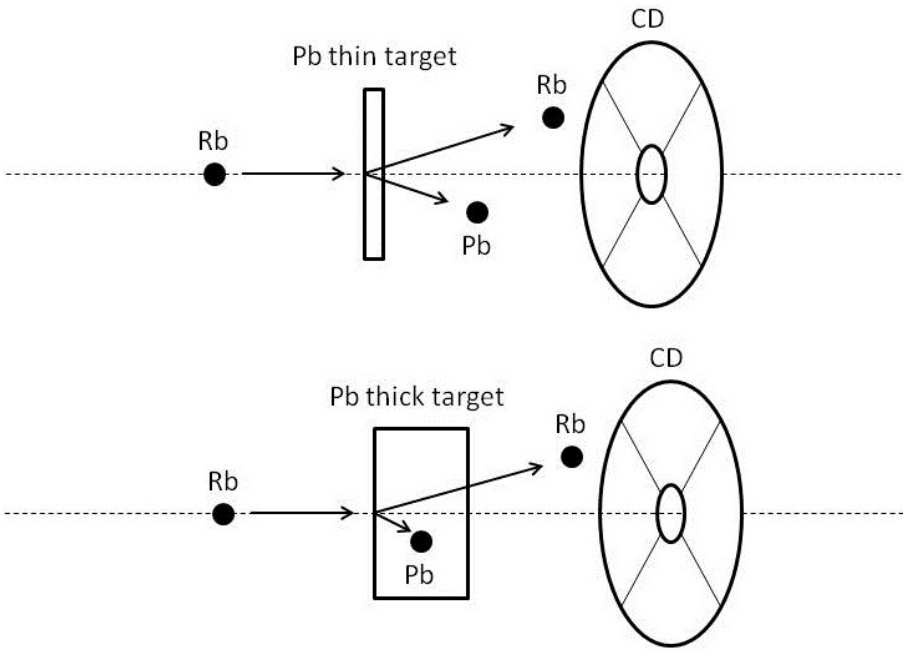

Figure 2.4: Schematic drawing of the Rb impinging on the Pb thin (top) and thick (bottom) targets.

The setup consisted of 8 MINIBALL clusters detectors mounted surrounding the target chamber and of a particle CD detector, which is made of 4 quadrants of double-sided-silicon-strip detector (DSSSD) [2]. The target chamber with the MINIBALL detectors and the CD are shown in figure 2.5.

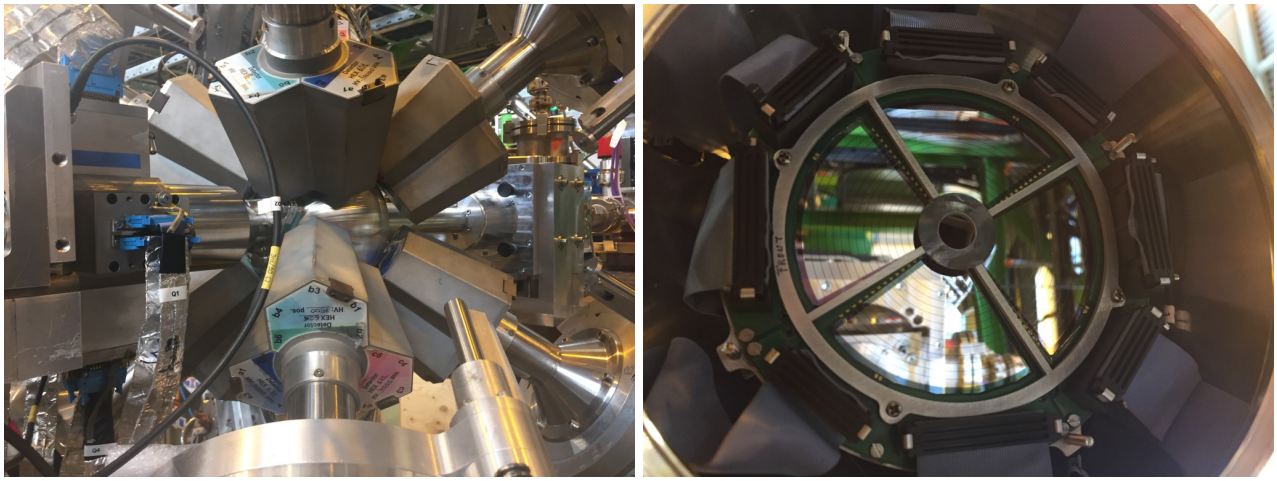

Figure 2.5: Left image: picture of the target chamber with the MINIBALL clusters. Right image: the particle CD detector. An absorber was mounted in the inner rings in order to reduce the Rutherford scattering and the damage in the detector.

The position of the CD was fixed in order to be as much sensitive as possible to the grazing angles of the rubidium-like particles that are linked to the lead-likes ones in which we are interested. The angles covered by the CD were between 30^o to 65^o.

Chapter 3

Pre-sorting of the data

Before starting with the analysis of the ^{94}Rb on ^{208}Pb data, it is important to perform some pre-analysis, like particle and gamma calibration, that have already been provided by the MINIBALL collaboration, or the γ efficiency. In the first section, the structure of the data and the experimental variables recorded will be specified. In the second section, the MINIBALL efficiency will be calculated. Then, due to the fact that the beam is not stable, various contaminant nuclei are present: the third section, "Contaminants", will discuss about them and how to deal with them.

3.1 Structure of the data

An aspect useful to know for the analysis is how the data were taken. The measurement was made in this way: when a bunch of ^{94}Rb reached the ^{208}Pb target, the data were stored for 1.6 ms, the so-called BEAM ON window; then, after waiting approximatively 0.5 ms for the collection of the data by the electronics, another 1.6 ms of data were stored without the beam, the so-called BEAM OFF window, useful for the background study; then another bunch arrived at the target after waiting 0.5 ms and the cycle continued in this way. The signal given by EBIS was useful to start the measurement at the right time.

During this experiment the γ rays were recorded all in triggerless mode. Instead, the particle detection was carried out in two ways, depending on the target used. For the thin target a triggerless mode was selected, however for the thick target the particles without any gamma in coincidence (a window coincidence of 800 ns was chosen) were downscaled in order to reduce the number of useless data accumulated. The segmentation of the detectors helped in the tracking reconstruction. The data stored were the energy, the time of arrival and the position of gammas and particles. In addition, the signal of the bunch arrival from EBIS was recorded.

3.2 The MINIBALL efficiency

An important property of the detectors is the so called "efficiency", which is related to the goodness in measuring the particles. It has to be said that not all the gammas emitted from a γ-ray source (that is, in this case, an excited nucleus) are detected: some of them are lost, for example because they do not fly through a detector or because the detector is unable to see them. A quantity related to this issue is the efficiency [4, 19]:

$$\epsilon = \frac{N_\gamma^{detected}}{N_\gamma^{emitted}}, \tag{3.1}$$

that is the ratio between the gamma particle detected and those produced by the source.

The efficiency varies with the energy and a detector works well in some energy ranges rather than others. It is important to correct with efficiency calculations the intensities of the gammas measured, in fact one can have lower intensity than normal for the fact that the energy of the gamma ray is in a range of energy where the detector has a poor efficiency. The relation between efficiency and intensity

is:

$$\epsilon = \frac{area\ of\ the\ peak}{activity \cdot time \cdot I_\gamma}, \tag{3.2}$$

where *area of the peak* means the area in the histogram of the peak of the transition of interest, *activity* is the activity of the unstable nucleus, *time* is the time of measurement and I_γ is the intensity of the transition. Using equation 3.2 it is possible to calculate the intensities of the various transitions knowing all the other quantities.

First of all, the efficiency has to be calculated measuring well known transitions with the detector that will be used in the experiment. To do this, ^{133}Ba and ^{152}Eu were put in the experimental chamber at the target position and their gamma rays were measured. The gamma energy histogram of this measurement is shown in figure 3.1.

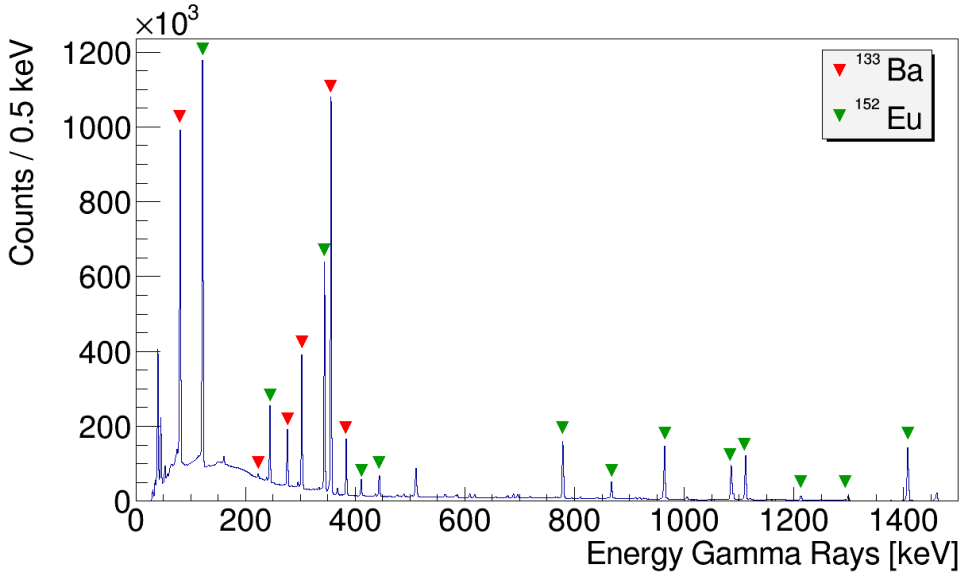

Figure 3.1: Gamma energy histogram of the efficiency-calibration measurement, performed with ^{133}Ba and ^{152}Eu. The ^{133}Ba transitions are highlighted by red triangles and the ^{152}Eu transitions are marked with green triangles.

The area of the peaks are calculated via fitting the peak with a gaussian function and removing the background subtracting it after a linear approximation. The activity is given by the decay law

$$A = A_0\ e^{-\lambda\, t}, \tag{3.3}$$

where A_0 is the activity measured in a certain moment (the values are 6.33(1) kBq for the Ba and 7.62(1) kBq for the Eu), t is the time between the moment of the A_0 measurement and when the two isotopes were used for the efficiency calibration (so the time between 01/04/16 and 01/09/17 that is 518(1) days for both the isotopes) and λ is the decay constant or

$$\lambda = \frac{ln2}{t_{1/2}}, \tag{3.4}$$

where $t_{1/2}$ is the time of halving of the unstable species (λ is $2.083(2)\cdot10^{-9}s^{-1}$ for the Ba and $1.626(1)\cdot10^{-9}s^{-1}$ for the Eu). Then, the *time* of the measurement was 9534.32(4) s and the intensities are tabulated. Table 3.1 shows the transitions energy, the intensities and the areas of the peaks of interest, all with their errors.

With these values the efficiency and its error were calculated and then fitted with the formula

$$ln(\epsilon) = \sum_{i=0}^{4} A_i (ln(Energy))^i, \tag{3.5}$$

where the A_i, with $i = 0, \ldots, 4$, are the five fit parameters. The result of the fit and the five parameters are shown in figure 3.2 and table 3.2.

	E_γ [keV]	I_γ [%]	Peak area [Counts]
^{133}Ba	80.8110(6)	36.7(3)	$3762(2)\cdot10^3$
	223.13(2)	0.450(4)	$46(1)\cdot10^3$
	276.371(2)	7.15(3)	$638(1)\cdot10^3$
	302.8063(9)	18.30(6)	$1543(1)\cdot10^3$
	355.9717(4)	61.9(1)	$4780(2)\cdot10^3$
	383.814(1)	8.91(3)	$677(1)\cdot10^3$
^{152}Eu	121.7367(5)	28.6(2)	$4334(2)\cdot10^3$
	244.622(1)	7.548(2)	$877(1)\cdot10^3$
	344.2566(6)	26.5(4)	$2647(2)\cdot10^3$
	411.079(3)	2.234(4)	$1915(8)\cdot10^2$
	443.919(3)	3.15(2)	$2582(6)\cdot10^2$
	778.821(1)	12.94(2)	$799(1)\cdot10^3$
	867.349(3)	4.25(3)	$2427(6)\cdot10^2$
	963.994(1)	14.61(2)	$8188(9)\cdot10^2$
	1085.905(2)	11.45(3)	$5653(8)\cdot10^2$
	1112.001(2)	13.64(2)	$6990(9)\cdot10^2$
	1212.851(7)	1.412(8)	$660(3)\cdot10^2$
	1299.085(6)	1.62(1)	$699(6)\cdot10^2$
	1407.881(1)	21.01(2)	$935(1)\cdot10^3$

Table 3.1: Transitions energy, intensities and areas of the peaks of interest, all with their errors.

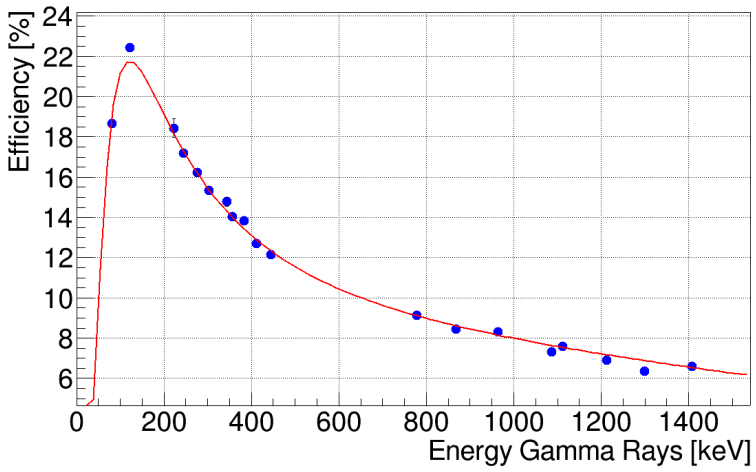

Figure 3.2: Graph showing the efficiency in percentage versus the gamma energy in keV.

Parameter	Value
A_0	-79(3)
A_1	54(2)
A_2	-1.3(6)
A_3	1.41(7)
A_4	$-5.6(3)\cdot10^{-2}$

Table 3.2: The five fit parameters.

After these efficiency calculations, it is possible to have the corrected transitions intensities of the nuclei detected with the MINIBALL detector.

3.3 Contaminants

One problem that deserves to be mentioned is the possibility to have other nuclei that disturb, namely contaminate, the gamma spectrum. The gamma rays emitted by these nuclei are not related to the reaction between beam and target. There are three main sources of contaminants gammas in this experiment, solved using different methods:

1. Nuclei coming from the decays of ^{94}Rb: radioactive ion beams are made of unstable nuclei that can change their nature by decaying into different nuclei. ^{94}Rb, maybe scattered and deviated by a nucleus in the target, can be implanted inside the chamber. It decays via β^- decay after 2.70 seconds into ^{94}Sr, that decays in its turn into ^{94}Y after 74 seconds and at the end this turns into the stable ^{94}Zr after 18.7 minutes. Therefore, the γ-rays associated to the β^- products are the major contaminants in the gamma spectra;
2. The ^{94}Rb decays while the beam is accelerated in the machine;
3. Due to the energy of the beam, higher than the coulomb barrier, different reactions can be observed, like: rutherford, coulomb excitation and other inelastic reactions. However, the coulomb excitation will produce a huge number of gamma rays that will hide the gammas of interest.

There are two main ways to take care of the background, that will be specified in section 4.2. The first one is to subtract the data taken when there was not the beam from the data taken when the beam bunch arrived at the target. Doing this the gammas coming from contaminants can be removed. The second is to take in consideration only the gamma rays detected in coincidence with a particle, so after a reaction, and to subtract a background of gammas coming from the random coincidences between particles and gammas.

Chapter 4

Data analysis and results

Two analysis will be presented in this chapter. In the first section, one of the contaminants, ^{94}Zr, will be analyzed because it is present in the major part of the γ spectra. After this section, the ^{210}Pb analysis will be performed. As it was said in section 2.3, two thicknesses were chosen for the experiment: all the data analysis in the following refers to the thicker one, namely the 13 mg/cm^2 target.

4.1 The ^{94}Zr analysis

In section 3.3 was pointed out that various contaminants are present when using radioactive beams. In this case, using a ^{94}Rb beam, the stable ^{94}Zr is one of the major contaminants and it disturbs the γ spectra. For this reason, 3 hours of background data were taken after the experiment in order to study the radiation produced due to the implantation of the beam inside the chamber. This radiation is dominated by the β^- decay chain of the beam, where the ^{94}Zr nucleus is the last element. Therefore, with the help of the level scheme previously studied by B. Singh et al. [20] and the background data, the level scheme of this nucleus will be revised. A $\gamma\gamma$ matrix is essential to study the ^{94}Zr via $\gamma\gamma$ coincidences. It is shown in figure 4.1.

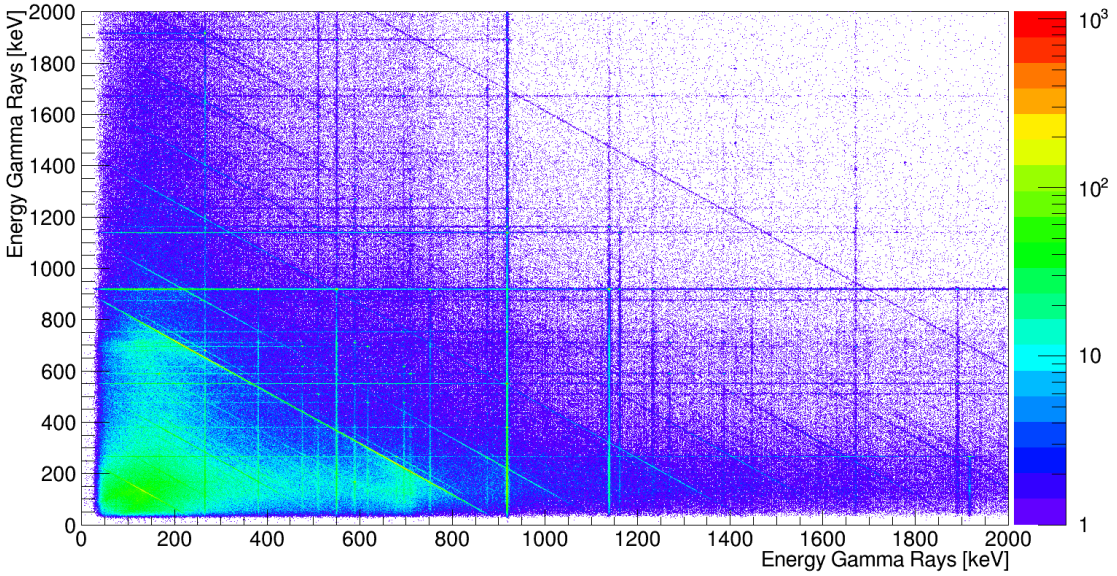

Figure 4.1: The ^{94}Zr $\gamma\gamma$ matrix used for the $\gamma\gamma$ coincidences.

The gamma decay analysis was performed via studying the gamma singles spectrum, shown in figure 4.2 (a), and the $\gamma\gamma$ matrix. The $\gamma\gamma$ coincidence analysis is explained in appendix B. The total projection of the matrix on one axis was used for selecting the gates. This projection, with some transitions highlighted, and two examples of coincidences are shown in figure 4.2 (b, c, d), specifically

the ones at 918 keV and 1671 keV. Gating on the transition at 918 keV, the lines in coincidence with it are clearly visible and marked as "certain" in the level scheme, as can be seen in figure 4.2 (c). For the case of the 1671-keV line, the 694-keV and 1236-keV lines are present and two new transitions at 386 keV and 1388 keV can be seen, referring again to figure 4.2 (d).

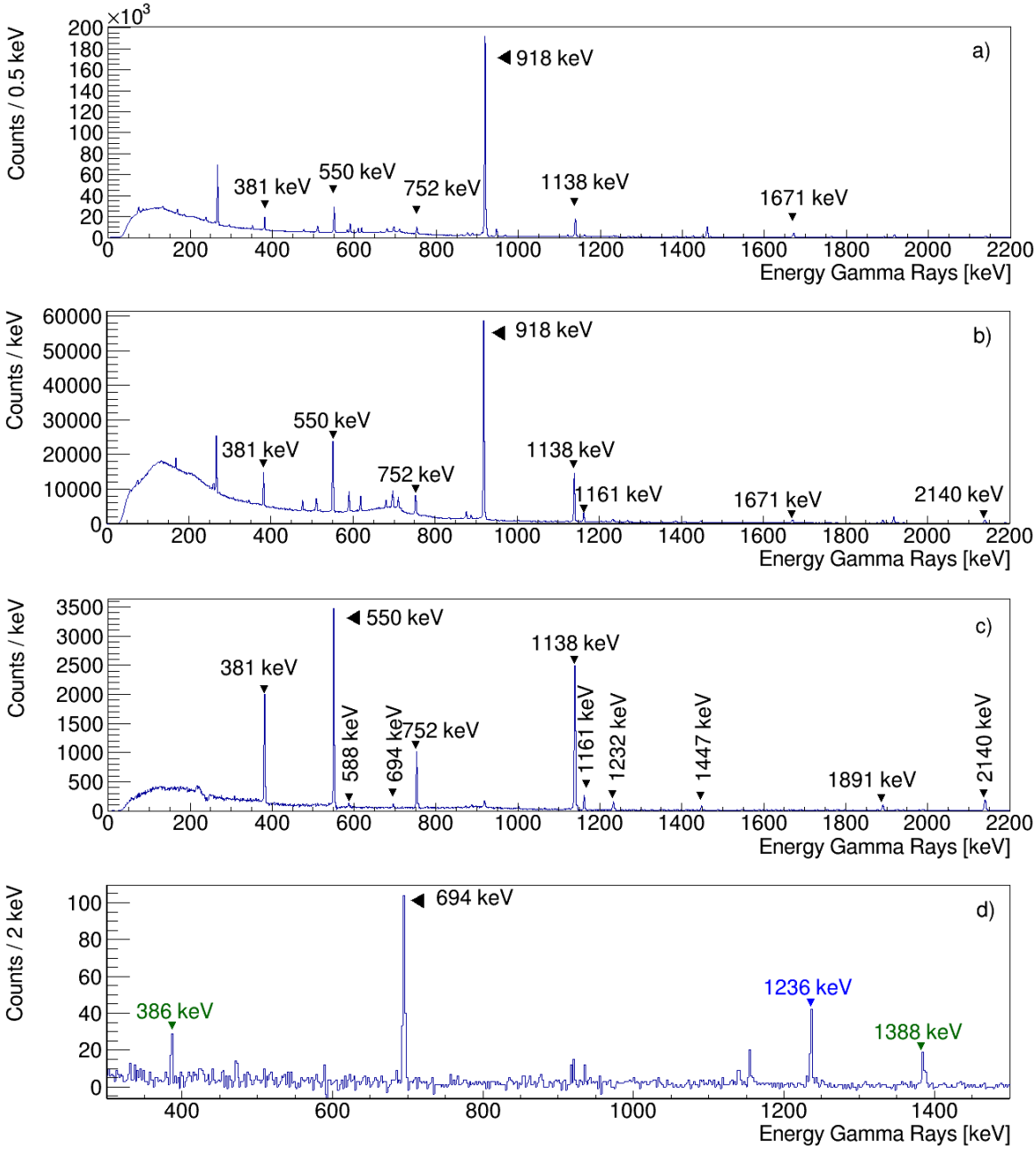

Figure 4.2: a) the ^{94}Zr singles spectrum; b) the total projection of the ^{94}Zr matrix; c) the gate on the 918-keV transition; d) the gate on the 1671-keV transition.

The transitions at 1236 keV, 1989 keV, 2255 keV, 2492 keV, 2527 keV, 2566 keV, 2661 keV and 2898 keV related to the 2908-keV, 3725-keV, 3962-keV, 4198-keV and 4237-keV states were firmly observed when previously they were only suggested. In addition, six new transitions were seen with an energy of 386 keV, 872 keV, 1388 keV, 1941 keV, 2348 keV and 3261 keV, and three uncertain transitions with energies of 759 keV, 1668 keV and 2637 keV. As a consequence, there are four clear new levels at 2930 keV, 3410 keV, 3818 keV and 4180 keV and another uncertain new level at 4107 keV. The final level scheme obtained after the analysis is shown in figure 4.3.

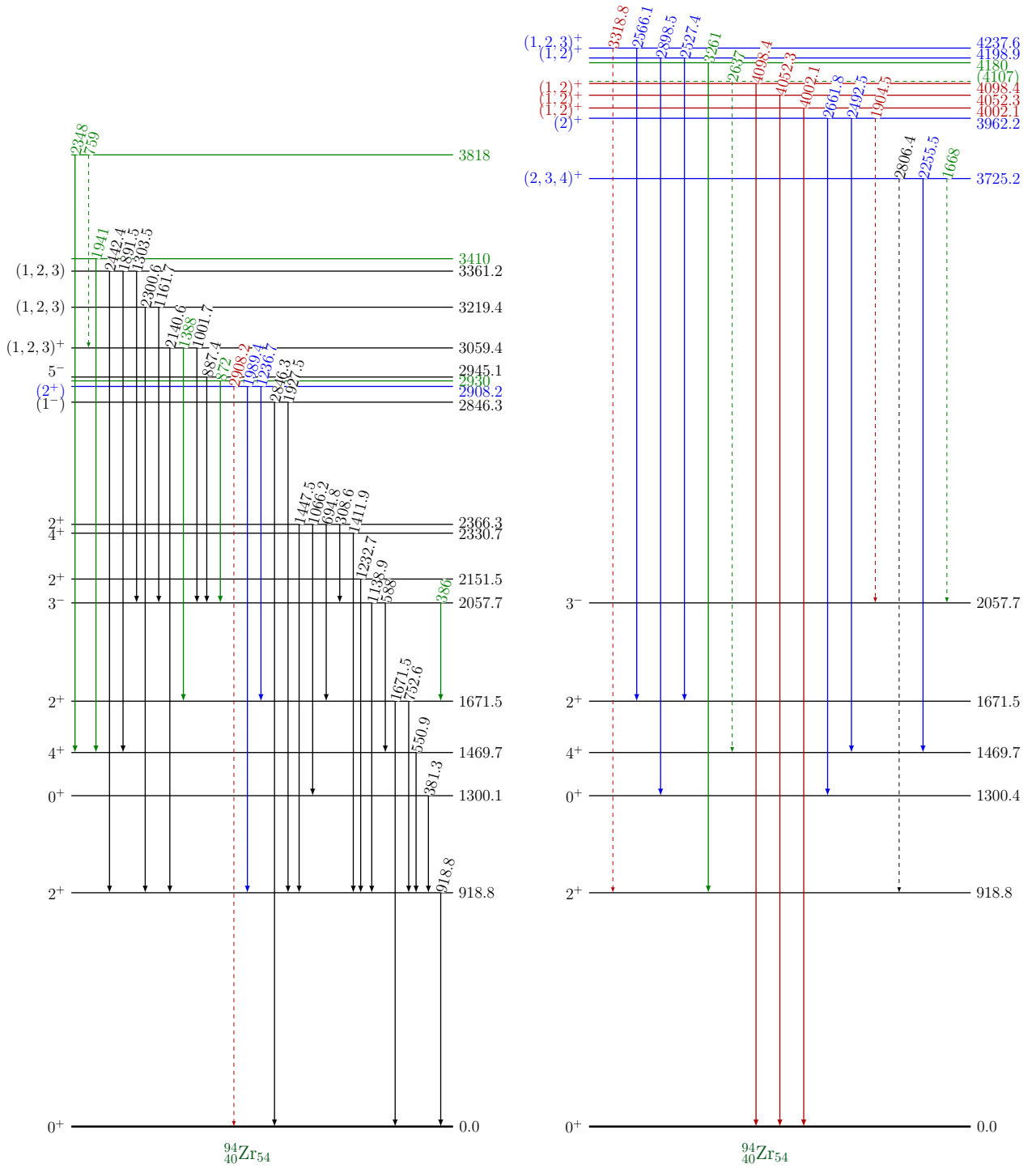

Figure 4.3: Level scheme of the ^{94}Zr obtained in this analysis. The horizontal lines are the levels and the numbers at their right are their energies: if a level line is continuous it means that the level is well established and if it is dashed that is uncertain. The values at the left are the total angular momenta and parity of that state: if it is in brackets it is uncertain. The vertical arrows are the transitions between the levels and the style continuous/dashed means the same as the levels. The color code is: black if it is present in the literature scheme and it was observed in the analysis; red if it is in the literature but it was not observed; blue if it is present in the literature but it was uncertain and it was observed with sureness; green if it was not present in the literature but was observed, meaning that a new level or transition was discovered.

4.2 The ^{210}Pb analysis

The first important spectrum for the ^{210}Pb analysis is the particle distribution, in which it is possible to identify the projectile- and target-like particles [21], as it is shown in figure 4.4. The number of particles with a specific energy and scattering angle are plotted. The different regions represent the Rb (the projectile), the Pb (the target) and some electronic noise.

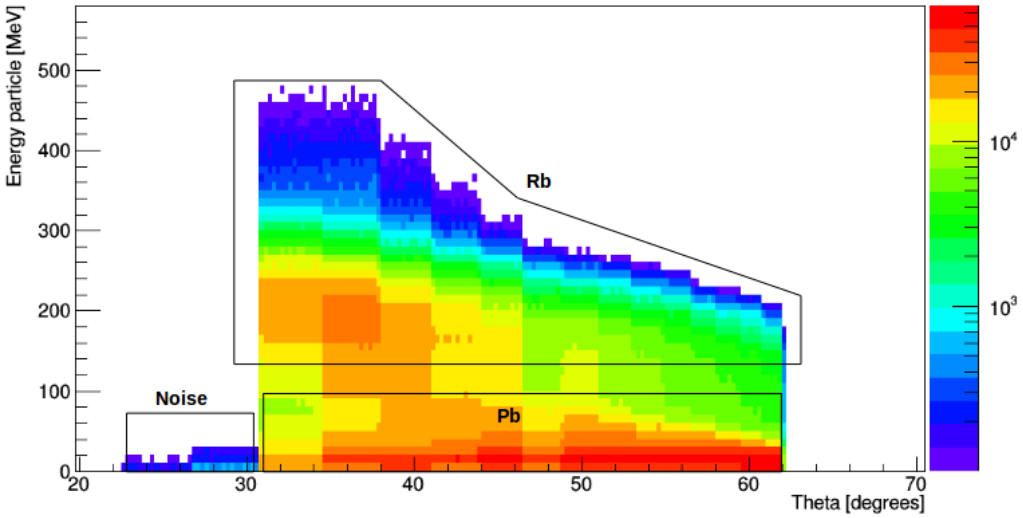

Figure 4.4: Particle distribution for the experiment. The regions represent the Rb and the Pb particles, and noise at low angles.

The gamma spectrum, without particle coincidence, is dominated by the X rays of the lead and the background, as can be seen in figure 4.5.

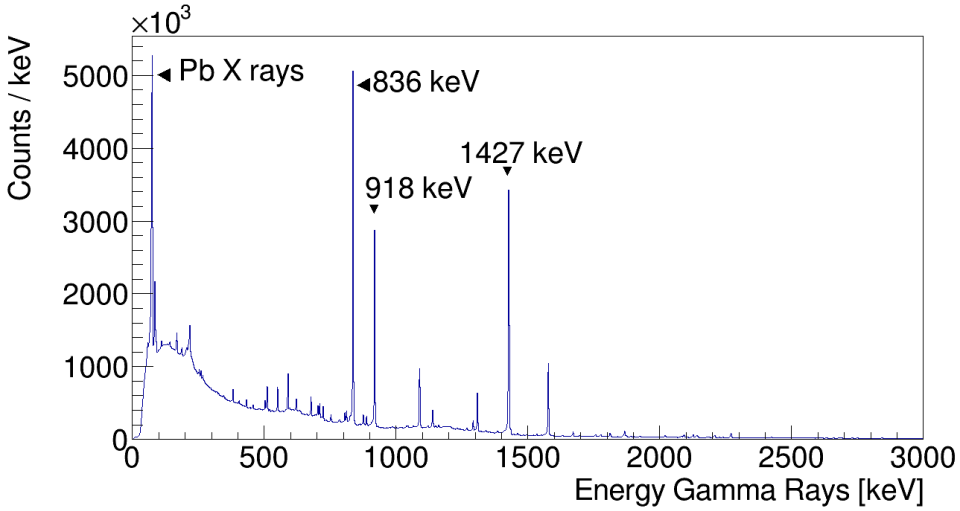

Figure 4.5: The γ spectrum without background subtraction. The high peaks are related to the background, like: ^{94}Sr (836 keV), ^{94}Zr (918 keV), ^{94}Y (1427 keV) and the X rays of the lead.

A way to clean the spectrum is to use the bunching of the beam, so the BEAM ON and BEAM OFF windows presented in section 3.1. Subtracting the BEAM OFF from the BEAM ON window data [22], the resulting histogram contains only the gammas of interest and those coming from short life states of the contaminants. In fact, if any contaminants long life state gamma was present, it would be removed by this subtraction since it would be present in both the histograms (it is needed to keep in mind that the bunches continued to hit the target and these long life states can decay in the BEAM ON window and in the BEAM OFF too).

Another method to remove the unwanted gammas is to perform a particle-γ coincidence [22, 21].

This method permits to exclude the gamma rays that are not related with a particle. Therefore, representing the time difference between the particles and the gammas it is possible to identify different regions associated to different cases, as it is shown in figure 4.6. The prompt region represents the particles that are in coincidence with the gammas, the p-γ coincidence, and the random region defines the aleatory, or random, coincidence between a particle and a gamma. This is caused by a rutherford-scattered particle and a gamma of the background. The last region, called delayed, represents all the gammas associated with a particle after an isomer state is fed [3]. The random part is present over the prompt and delayed regions, therefore in order to have only the gammas related with the reactions a subtraction of the background is mandatory before continuing with the analysis. An example of how looks like the gamma spectrum after this background reduction, for the prompt part, is shown in figure 4.7. As can be seen in this figure, the only gammas that remain are related to the coulomb excitation lines of ^{94}Rb at 214 keV and several lines between 300 keV and 500 keV, ^{94}Sr at 836 keV, ^{208}Pb at 2614 keV, the MNT lines and the X rays from the target.

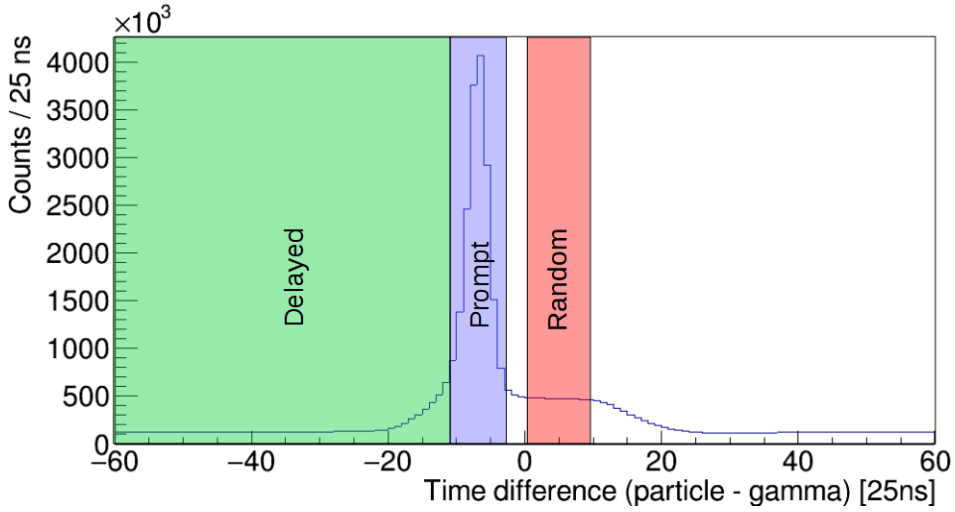

Figure 4.6: Time difference between the particles, t_p, and the gammas, t_γ. In the green region there are the delayed gammas, in the blue area there are the prompt gammas and the the red region there are the random gammas.

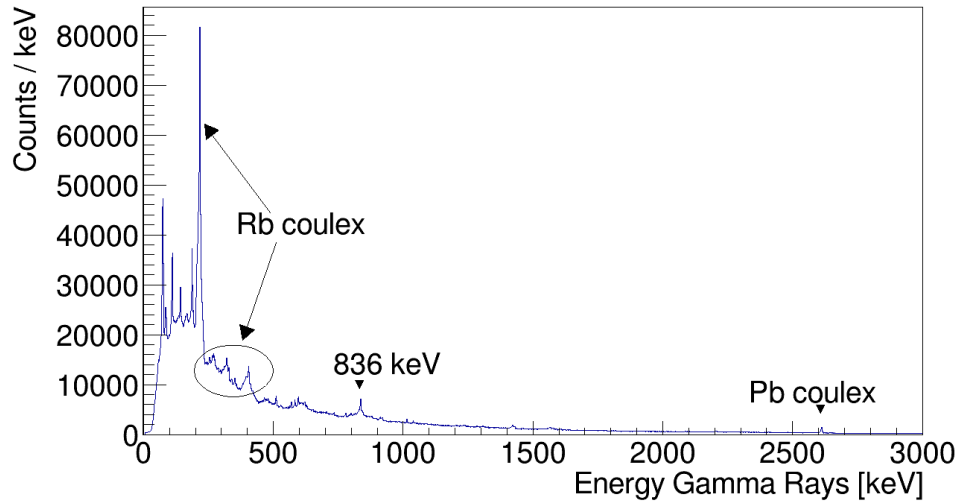

Figure 4.7: Histogram representing the counts of the gamma energy with background reduction. The high peaks related to the background are clearly reduced. The ^{94}Rb coulex, ^{94}Sr 836-keV and Pb coulex transitions are shown.

4.2.1 Level scheme

The γ-single and the $\gamma\gamma$-coincidence analysis were also performed for ^{210}Pb. However, this nucleus has isomer states and for this reason more than one matrix is needed: the three prompt-prompt, prompt-delayed and delayed-delayed matrices were constructed in order to establish a complete level scheme. As an example of these matrices, the prompt-delayed case is shown in figure 4.8. In addition, in figure 4.9 the projections of the two axes of the prompt-delayed matrix are presented. The transitions at 297 keV, 799 keV, 528 keV and 1233 keV of the ^{210}Pb are marked.

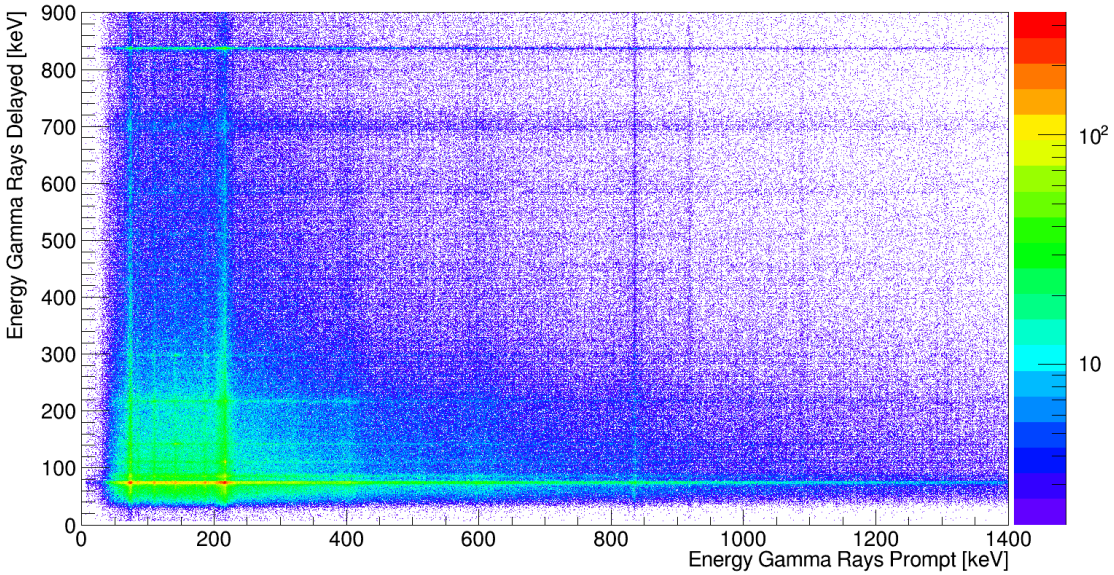

Figure 4.8: The prompt-delayed matrix used for the ^{210}Pb analysis.

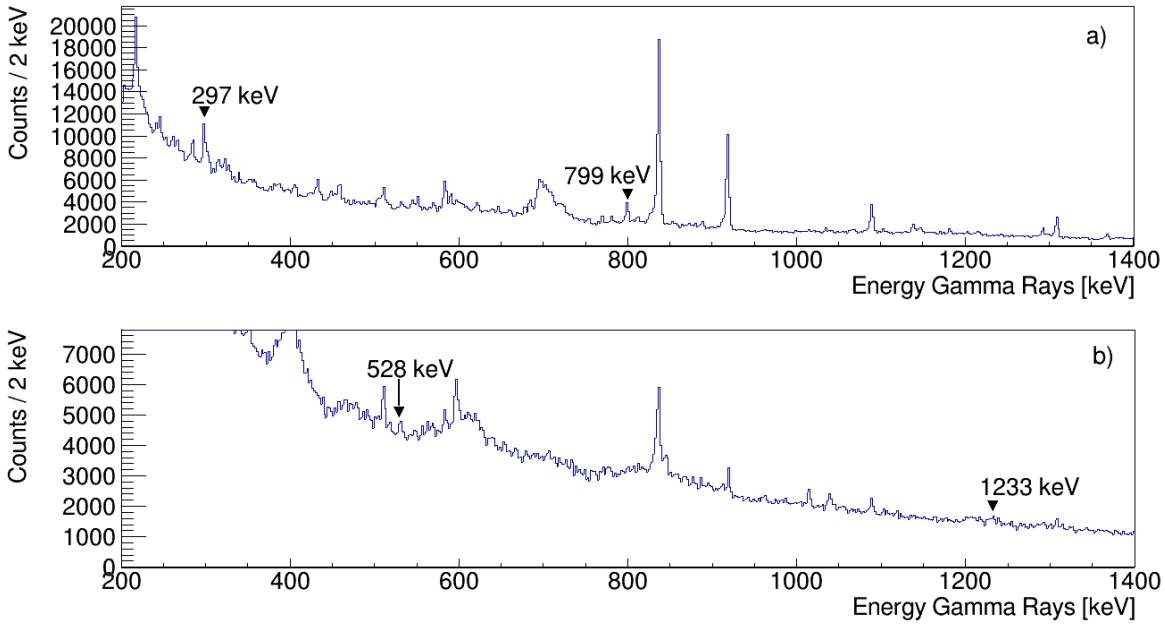

Figure 4.9: The delayed total projection (a) and the prompt total projection (b) of the prompt-delayed matrix.

Due to the fact that the states at 1194 keV and at 1274 keV are both isomer levels, the transitions above the 1274-keV level are prompt and the ones under it are delayed, hence the only two lines in coincidence after the isomer states are the 297-keV and 799-keV lines. In order to extract all the information about ^{210}Pb, several gates using the different matrices were performed and some of them are shown in figure 4.10. Two lines at 640 keV and 1346 keV associated with states above the isomer at 1274 keV were found during the analysis.

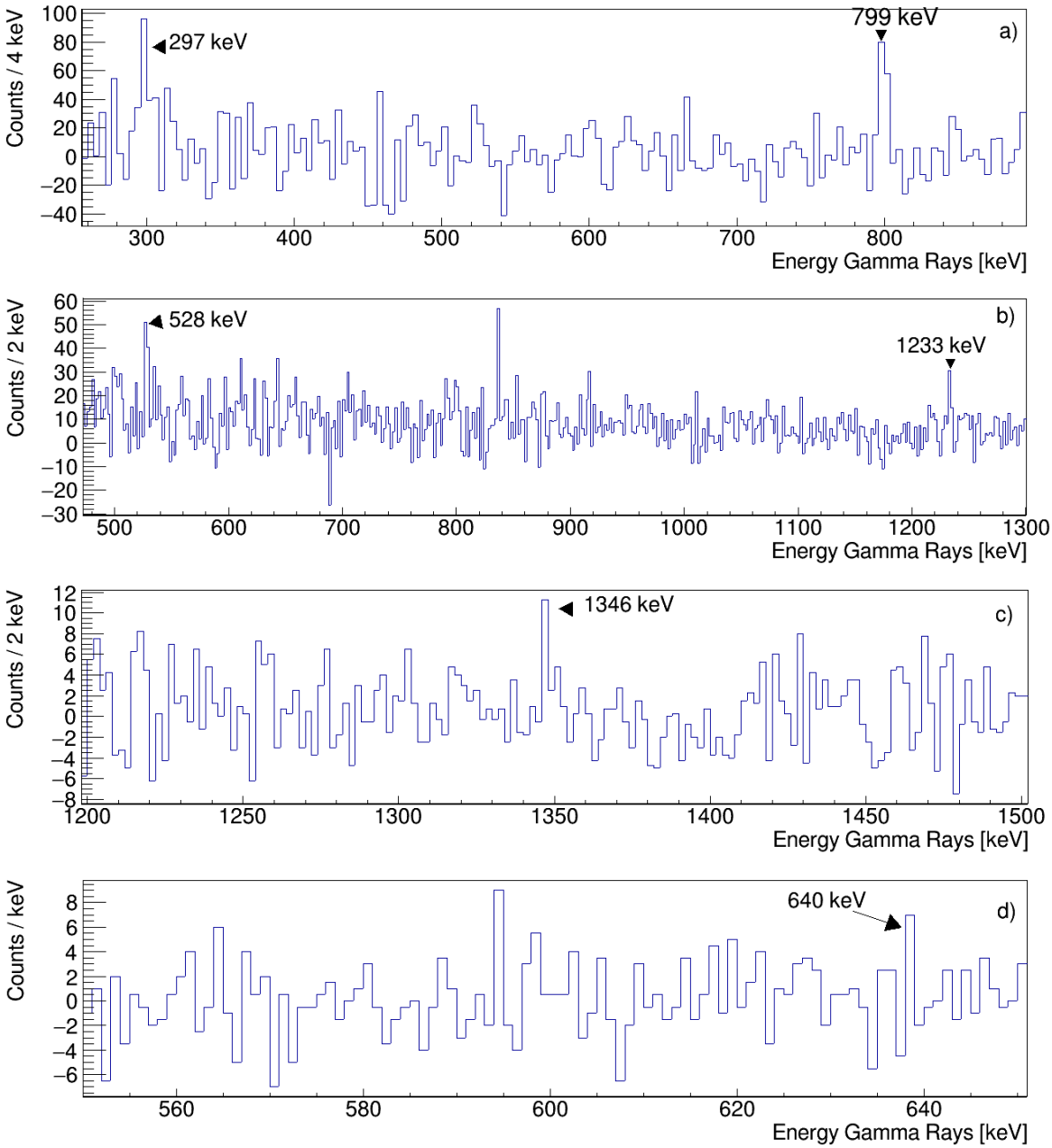

Figure 4.10: a) sum of the histograms of the delayed-delayed coincidence of the 297-keV and 799-keV gates; b) sum of the histograms of the delayed-prompt coincidence of the 297-keV and 799-keV gates; c) 528-keV prompt-prompt coincidence; d) 1233-keV prompt-prompt coincidence.

The level scheme followed to do the $\gamma\gamma$ coincidences is shown in the left image of figure 4.11. Instead, the level scheme of the ^{210}Pb constructed combining all the information of the γ singles spectra and the $\gamma\gamma$ coincidences is shown in the right image of figure 4.11.

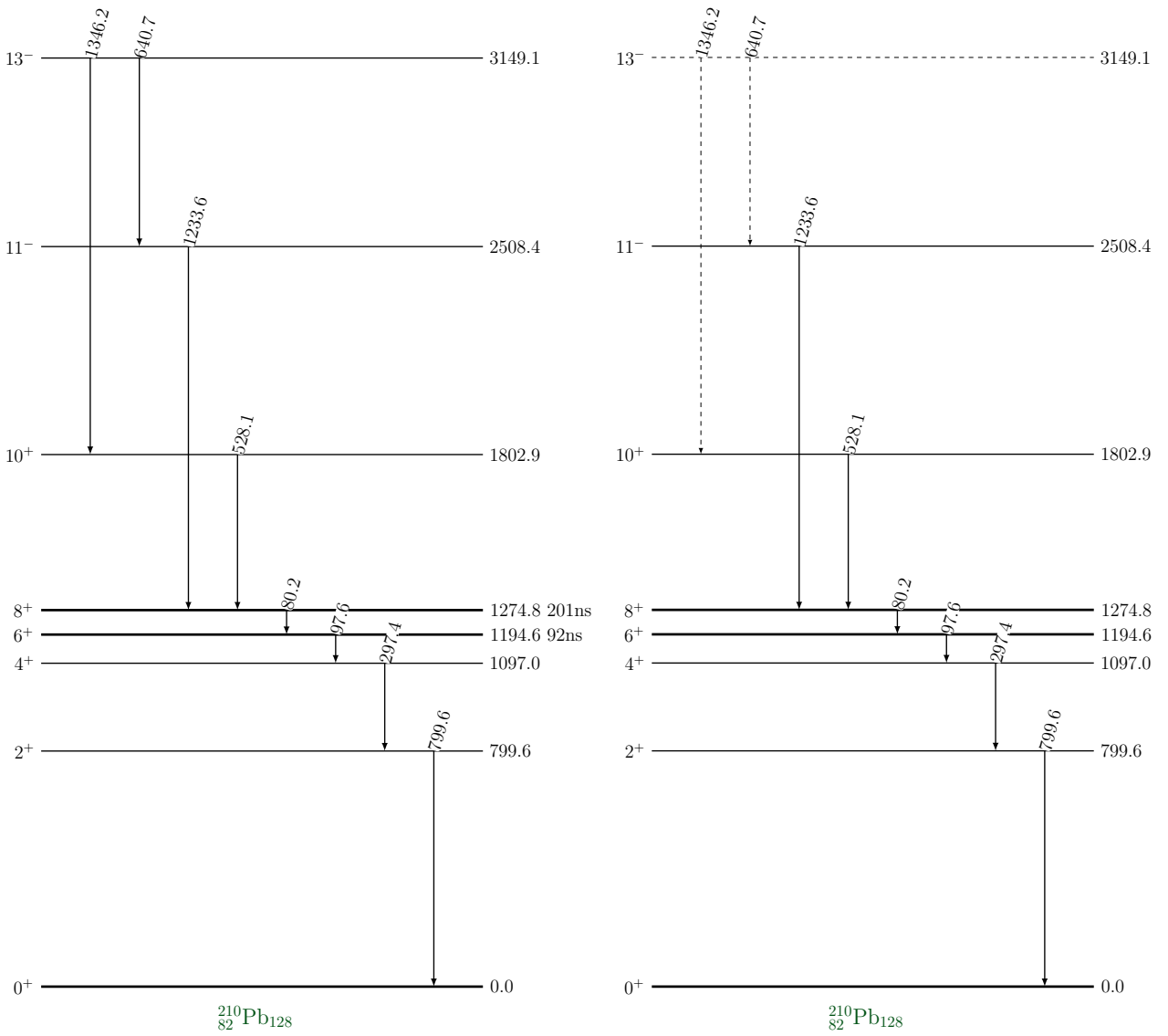

Figure 4.11: Left image: partial level scheme for $^{210}_{82}Pb_{128}$, taken from [23]. Right image: final level scheme extracted from the data of this experiment. The meaning of the lines and colors is the same than figure 4.3. Here there are also isomer levels, recognizable by a thicker continuous line and the lifetime is shown at the right of the energy.

4.2.2 Shell model calculations

In this section the experimental results will be compared with the shell model predictions [24, 25, 26]. Within this model, the ^{210}Pb is described with a ^{208}Pb inert core, since the ^{208}Pb is a doubly-magic nucleus with Z = 82 and N = 126. The two excited neutrons are positioned in the states above the N = 126 shell gap, as can be seen in figure 1.3. The valence space that was used in the calculations is given by ($g_{9/2}$, $i_{11/2}$, $d_{3/2}$, $d_{5/2}$, $g_{7/2}$, $s_{1/2}$, $j_{15/2}$), where the $j_{15/2}$ shell is an intruder state with negative parity. Consequently, the properties of the ^{210}Pb, like the energies of the excited states, are given by the two neutrons above the shell gap.

The results of the calculations with the shell-model code ANTOINE [27, 28] using the Kuo-Herling (KH) interaction [29] give the following occupation numbers:

1. for the 0^+, 2^+, 4^+, 6^+, 8^+ states the two neutrons are mostly in $g_{9/2}$
2. for the 10^+ state approximatively one neutron is mostly in $g_{9/2}$ an one mostly in $i_{11/2}$
3. for the 11^- state approximatively one neutron is mostly in $g_{9/2}$ an one mostly in $j_{15/2}$
4. for the 13^- state approximatively one neutron is mostly in $i_{11/2}$ an one mostly in $j_{15/2}$

Furthermore, as can be seen in figure 4.12, the predicted energies are in agreement with the experimental results.

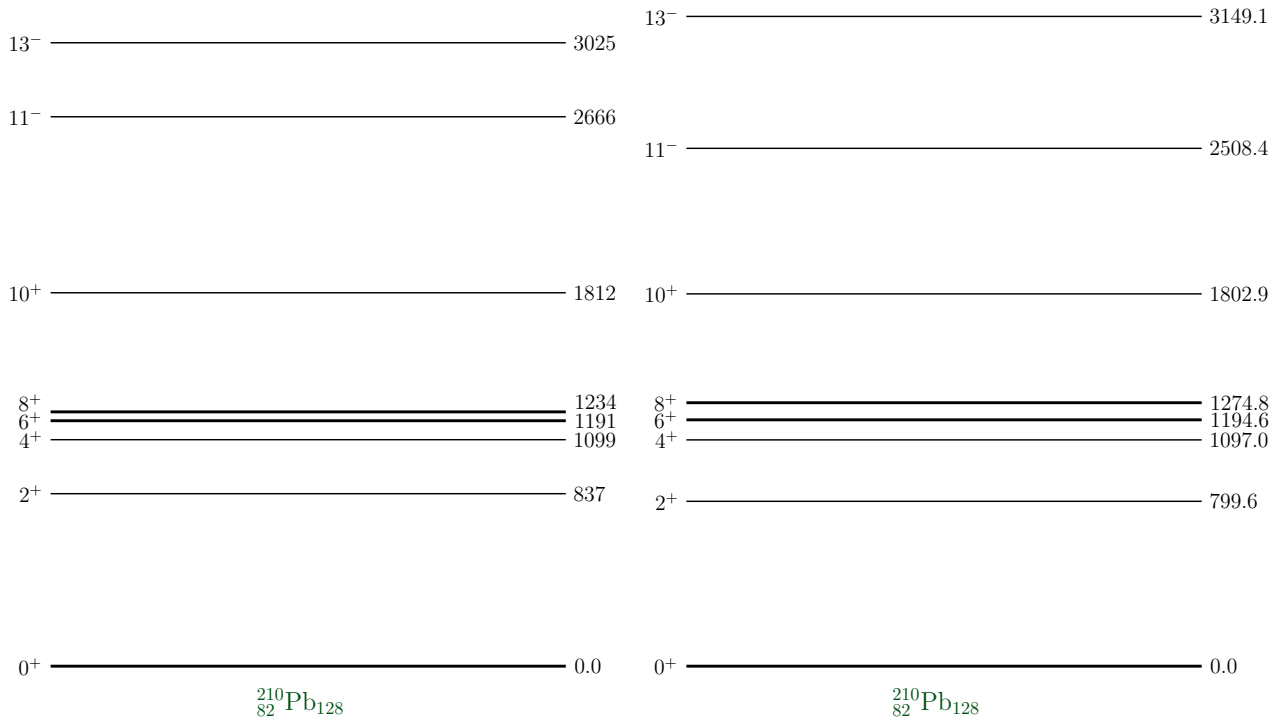

Figure 4.12: Experimentally deduced level scheme for the ^{210}Pb (right), compared with ($g_{9/2}$, $i_{11/2}$, $d_{3/2}$, $d_{5/2}$, $g_{7/2}$, $s_{1/2}$, $j_{15/2}$) shell-model calculations with the Kuo-Herling interaction (left).

Chapter 5

Conclusions and future perspectives

This thesis is devoted to the gamma-ray spectroscopy study of ^{210}Pb and ^{94}Zr populated via a multi-nucleon transfer reaction with a ^{94}Rb radioactive ion beam impinging on a ^{208}Pb target. The experiment was performed on September 2017 at ISOLDE, CERN, using the MINIBALL setup together with a silicon detector for particle tagging. A detailed analysis of the experimental data was performed by using the $\gamma\gamma$ coincidences technique in order to build up the level schemes of ^{210}Pb and ^{94}Zr. Since the ^{210}Pb presents isomers of some hundred picoseconds in its structure, it was necessary to perform prompt-delayed, delayed-delayed and prompt-prompt $\gamma\gamma$ coincidences in order to build up the levels below and above the 6^+ and 8^+ isomers. The experimental level scheme deduced for ^{210}Pb was compared with shell model calculations obtained with the code ANTOINE and using the Kuo-Herling interaction. The agreement of the theoretical calculations is excellent with the experimental results. The wave function of the studied states are also discussed within the thesis. The level scheme of ^{94}Zr is discussed in detail, emphasizing some of the improvements made with respect to the previously known level schemes in literature.

Within this thesis are not discussed the lifetime measurements of the isomeric states that can elucidate further the nature of the excited states in ^{210}Pb, this study will follow. Finally, the experiment described in this thesis will be repeated with a higher ^{94}Rb beam intensity of 10^7 pps, unlike the 10^6 pps intensity used in September 2017. This higher intensity will provide more statistics for the transitions already discussed in this thesis but more importantly it will be possible to reach more exotic nuclei, such as ^{212}Pb.

Appendix A

Interaction of gamma particles with matter

There are three main processes in the interaction photons-matter. Depending on the energy of the gamma, one among the three can overcome the other two. These three are, going up with the energy: photoelectric effect, Compton scattering and pair production. The photoelectric effect consists in an absorption of a gamma particle by an atom that emits as a consequence one of its electrons, if the energy of the photon overcomes the binding energy of the electron: this reaction has a role in the gamma-matter interaction until energies of 400-500 keV. Then, the following process is between some hundreds of keV and 5-7 MeV: the Compton scattering, namely a collision of the photon on a free electron that varies the energy and momentum of both particles. The last process is the pair production that can happen only if the energy of the gamma is at least 1.022 MeV, that is the sum of the rest masses of an electron and a positron. In fact, in this process the gamma ray interacts with the electromagnetic field of an atom and it disappears creating a pair of these two particles. The following figure A.1 shows the number of protons Z of the atom of the material versus the gamma energy E_γ (in MeV and logarithmic scale).

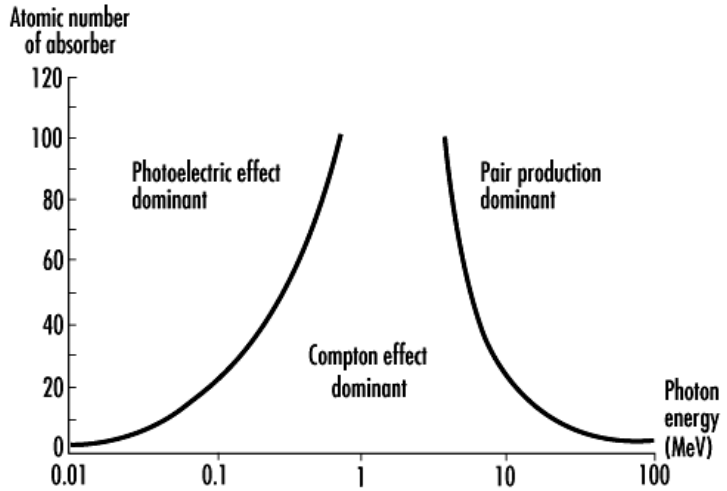

Figure A.1: Number of protons, Z, versus energy of the gamma, E_γ (in MeV and logarithmic scale). The regions where the different types of interaction between a gamma particle and matter are predominant are shown. Image taken from [30].

A gamma particle deposits its energy in the material following the different processes already explained. The gamma detectors use this principle to reconstruct the energy deposit, via collecting the electrons produced and converting the signals into energy informations.

Appendix B

How to do $\gamma\gamma$ coincidence analysis

The $\gamma\gamma$ coincidence method means choosing a gamma ray and finding the photons emitted in coincidence with that one. If a high energy state is reached after the reaction, multiple photons can be required to go from it to the bottom state with zero energy (taking the configuration where all the nucleons are in their least energy state as zero of the energy). Then, if the lifetime of the state is low enough, the photons are seen as subsequent, namely a gamma ray is emitted as soon as a state is reached after a transition.

From the point of view of the level scheme, it is possible to choose a transition and to see the gammas in coincidence with it. Figure B.1 shows an example on a level scheme of a dummy ${}^{A}_{Z}X_{N}$ nucleus. The horizontal lines are the quantum levels, the numbers at the right are the energies of them and the arrows are the transitions.

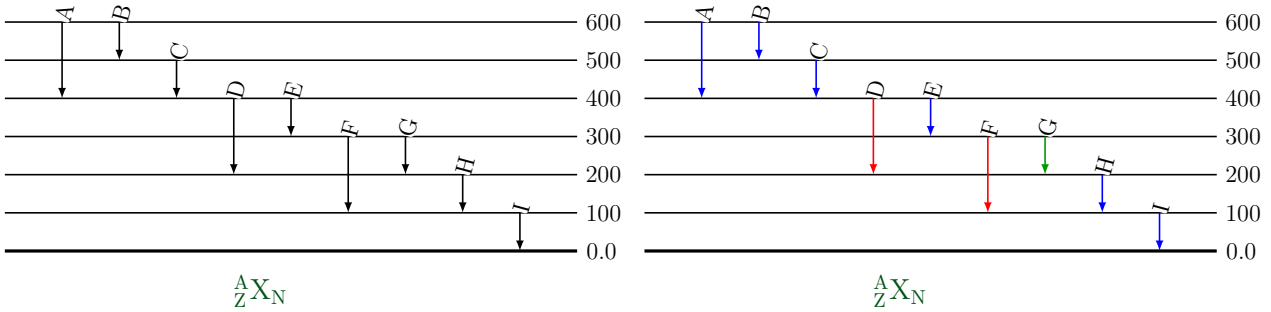

Figure B.1: Left image: dummy level scheme of a ${}^{A}_{Z}X_{N}$ nucleus with a few transitions. Right image: gating on the green transition G, the blue transitions A, B, C, E, H, and I are visible in coincidence with it. Instead, the red ones D and F are not in coincidence with G.

A coincidence with a transition, or in other words gating on a transition, now means choosing a transition of the level scheme of the nucleus under study and understanding which other transitions would be visible in coincidence with it. When a transition between an higher-energy level X and a lower-energy level Y is chosen to do the coincidence, the gammas in coincidence with it are those associated with transitions that fill the level X (even if not directly) or come from the level Y (even if not directly). Referring at figure B.1, if the transition G (colored in green in the figure) is the one chosen, the transitions A, B, C, E (that fills directly the state at 300 keV), H (that comes directly from the level at 200 keV), and I are in coincidence with it and are colored in blue in the figure. Instead, the red-colored transitions D and F are not in coincidence with G, because they do not finish on the 300-keV nor come from the 200-keV states. If some transitions were between eventual levels between 200 keV and 300 keV, they would not be seen (and neither, in general, all the transitions involving these possible states).

From the point of view of the data, finally, after looking at the predicted level scheme (needed to have a path to follow to do the various passages logically and not randomly), the total projections have to be watched and from them a peak at the right energy has to be chosen as transition (in terms of bins) and in consequence the background near it. Then, a projection of one of the axes in correspondence to the range of energy chosen in the other axes is performed, both for the peak and

the background. After this, the histogram taken as the background is subtracted from the histogram taken as the transition peak: this should enable the visualization of the transitions in coincidence with the one chosen. The word "should" is used because the most of the times several changes on the energy ranges chosen are needed to improve the final histogram. Furthermore, it is not sure that all the supposed transitions are present: if the statistics are too low, the coincidence peaks will not be seen. If all the coincidence peaks (or some of them, possibly the ones with the highest intensities) are visible gating on a transition, they and the states related to them can be drawn in the level scheme.

Bibliography

[1] J. J. Valiente-Dobon et al. Study of shell evolution around the doubly magic ^{208}Pb via a multinucleon transfer reaction with an unstable beam. Technical Report CERN-INTC-2013-015. INTC-P-379, CERN, Geneva, May 2013.

[2] A. Illana et. al. In-beam γ-ray spectroscopy of the first multi-nucleon transfer experiment performed with radioactive ion beams at HIE-ISOLDE. *INFN-LNL Report*, 251:40 – 41, 2018.

[3] J. J. Valiente-Dobon. Gamma-Ray Spectroscopy of Neutron-Rich Nuclei Populated via Multinucleon-Transfer Reactions. *Springer Proc. Phys.*, 182:87–111, 2016.

[4] William R. Leo. *Techniques for Nuclear and Particle Physics Experiments - 2nd edition.* Springer-Verlag Berlin Heidelberg, 1994.

[5] Otto Haxel, J. Hans D. Jensen, and Hans E. Suess. On the "Magic Numbers" in nuclear structure. *Physical Review*, 75:1766–1766, Jun 1949.

[6] *http://physics-database.group.shef.ac.uk/phy303/phy303-3.html.*

[7] M. Goeppert-Mayer. On closed shells in nuclei I. *Physical Review*, 74:235–239, Aug 1948.

[8] M. Goeppert-Mayer. On closed shells in nuclei. II. *Physical Review*, 75:1969–1970, Jun 1949.

[9] Kenneth S. Krane. *Introductory Nuclear Physics - 2nd edition.* John Wiley & Sons, Inc., 1988.

[10] M. Goeppert-Meyer and J. D. H. Jensen. *Elementary Theory of Nuclear Shell Structure.* John Wiley and Sons Inc., 1955.

[11] A. Bohr and B. R. Mottelson. *Nuclear Structure, Vol. I: Single-Particle Motion.* World Scientific Publishing, 1998.

[12] G.R. Satchler. *Introduction to Nuclear Reactions.* The Macmillan Press LTD, 1980.

[13] REX-ISOLDE. Homepage of the REX-ISOLDE Post-Accelerator. *http://isolde.web.cern.ch/isolde/REX-ISOLDE/index.html.*

[14] ISOLDE. Homepage of the HIE-ISOLDE Project. *http://hie-isolde-project.web.cern.ch/.*

[15] M. J. G. Borge and K. Riisager. Hie-isolde, the project and the physics opportunities. *The European Physical Journal A*, 52(11):334, Nov 2016.

[16] ISOLDE. Homepage of the ISOLDE facility. *http://isolde.web.cern.ch/isolde.*

[17] ISOLDE. Homepage of the MINIBALL detector. *http://isolde.web.cern.ch/experiments/miniball.*

[18] N. Warr et al. The miniball spectrometer. *The European Physical Journal A*, 49(3):40, Mar 2013.

[19] Glenn F. Knoll. *Radiation Detection and Measurement - 3rd edition.* John Wiley & Sons, Inc., 2000.

[20] B. Singh et al. A study of the gamma radiation from the decay of 94 y. *Journal of Physics G: Nuclear Physics*, 2(6):397, 1976.

[21] P. Colovic et. al. Study of the neutron-rich region in the vicinity of ^{208}Pb via multinucleon transfer reactions. *INFN-LNL Report*, 251:32 – 33, 2018.

[22] W.N. Catford et al. High resolution gamma-ray spectroscopy with a radioactive beam. *Nuclear Instruments and Methods in Physics Research Section A: Accelerators, Spectrometers, Detectors and Associated Equipment*, 371(3):449 – 459, 1996.

[23] R. Broda et al. Two-neutron and core-excited states in ^{210}Pb: Tracing $e3$ collectivity and evidence for a new β-decaying isomer in ^{210}Tl. *Phys. Rev. C*, 98:024324, Aug 2018.

[24] A. Gottardo et al. New Isomers in the Full Seniority Scheme of Neutron-Rich Lead Isotopes: The Role of Effective Three-Body Forces. *Physical Review Letters*, 109(16):162502, oct 2012.

[25] A.P. Zuker. *Large scale shell model calculations: The physics in and the physics out*, volume 482 of *Lecture Notes in Physics*. Springer Berlin Heidelberg, , 1997.

[26] H. Grawe and M. Lewitowicz. Shell structure of nuclei far from stability. *Nuclear Physics A*, 693(1-2):116 – 132, 2001.

[27] E. Caurier and F. Nowacki. *Acta Physica Polonica*, 30, 1999.

[28] E. Caurier et al. *Reviews of Modern Physics*, 77, 2005.

[29] E. K. Warburton and B. A. Brown. Appraisal of the kuo-herling shell-model interaction and application to a=210–212 nuclei. *Phys. Rev. C*, 43:602–617, Feb 1991.

[30] Workplace Health and Safety Information. *http://www.ilocis.org/documents/chpt48e.htm*.